Journal of Electrochemistry

Volume 24
Issue 6 *Special Issue in Honor of Professor Baolian Yi on His 80th Birthday*

2018-12-28

Facile Synthesis of Pt-Cu Alloy Nanodendrites as High-Performance Electrocatalysts for Oxygen Reduction Reaction

Liu-xuan LUO

Guang-hua WEI

Shui-yun SHEN

Feng-juan ZHU

Chang-chun KE

Xiao-hui YAN

Jun-liang ZHANG
Institute of Fuel Cells, School of Mechanical Engineering, MOE Key Laboratory of Power & Machinery Engineering;, junliang.zhang@sjtu.edu.cn

DOI: 10.13208/j.electrochem.180856 **Artical ID**:1006-3471(2018)06-0733-07
Cite this: *J. Electrochem.* **2018**, *24*(6): 733-739 **Http**://electrochem.xmu.edu.cn

Facile Synthesis of Pt-Cu Alloy Nanodendrites as High-Performance Electrocatalysts for Oxygen Reduction Reaction

LUO Liu-xuan[1], WEI Guang-hua[2], SHEN Shui-yun[1], ZHU Feng-juan[1],
KE Chang-chun[1], YAN Xiao-hui[1], ZHANG Jun-liang[1*]
(1. *Institute of Fuel Cells, School of Mechanical Engineering, MOE Key Laboratory of Power & Machinery Engineering*; 2. *SJTU-Paris Tech Elite Institute of Technology, Shanghai Jiao Tong University, Shanghai* 200240, *China*)

Abstract: Structures and compositions have significant effects on the catalytic properties of nanomaterials. Herein, a facile etching-based method was employed to synthesize Pt-Cu nanodendrites (NDs) with uniform and homogeneous alloy structures for enhancing oxygen reduction reaction (ORR). The formation of dendritic morphology was ascribed to the etching effect caused by the oxidative etchants of the Br^-/O_2 pair. The atomic ratio of Pt/Cu in Pt-Cu NDs could be easily tuned by altering the ratio of the Pt/Cu precursors, without deteriorating the dendritic morphology. The most active carbon-supported Pt_1Cu_1 NDs (Pt_1Cu_1 NDs/C) exhibited the area-specific activity of 1.17 $mA \cdot cm^{-2}$@0.9 V (vs. RHE), which is ~5.32 times relative to that of commercial Pt/C. Moreover, Pt_1Cu_1 NDs/C also possessed a remarkable electrochemical durability, preserving its superior ORR catalytic activity even after 12000 potential cycles during the accelerated degradation test. Such excellent catalytic activity and electrochemical durability of Pt_1Cu_1 NDs/C toward ORR were resulted from the combined electronic and structural effects, which are imparted by the Pt-Cu alloy structure and the dendritic morphology.

Key words: Pt; alloy; electrocatalysts; nanodendrites; oxygen reduction reaction
CLC Number: O646 **Document Code**: A

Over the past decades, hydrogen-based proton exchange membrane fuel cells (PEMFCs) have attracted tremendous attention as the promising alternatives to the traditional fossil-fuel-based energy conversion devices, due to their high efficiencies and low emissions, as well as the increasing concerns on the depletion of fossil fuel resources and the consequent environmental pollution[1-4]. Oxygen reduction reaction (ORR) in the cathode of PEMFCs is the rate-determining reaction, however, its sluggish kinetics, even on the state-of-the-art Pt/C, is still the main obstacle to the practical application of PEMFCs[1-3]. In addition, the electrochemical durability of Pt/C is also unsatisfactory under the acidic operating conditions of PEMFCs[5].

Engineering the structure and composition of nanomaterials has shown great potential in improving their catalytic properties[1, 3, 6-8]. Alloying Pt nanomaterials with foreign metals, synthesizing shape-controlled Pt-based nanomaterials and fabricating nanomaterials with core@Pt-shell structures have already been three most effective strategies to enhance the ORR catalytic properties of Pt-based electrocatalysts[1, 4, 6-10]. It is worth noting that, intense researches have been made for synthesizing the Pt-based nanomaterials with dendritic morphologies in recent years, showing greatly enhanced ORR catalytic properties[11-15]. Such enhancements in ORR catalytic properties are mainly attributed to the unique dendritic and alloyed structures, which can modify the exposed facets and electronic structures of the dendritic nanomaterials[11].

In this work, a facile etching-based method was applied to synthesize Pt-Cu nanodendrites (NDs) with

Received: 2018-09-28, Revised: 2018-10-29 *Corresponding author, Tel: (86-21)34207439, E-mail: junliang.zhang@sjtu.edu.cn

uniform size and morphology. The synthetic mechanism of Pt-Cu NDs was exploited, as well as their physicochemical properties. Due to the combined effects of the increased surface strain, modified electronic structure and active {111} facets, the most active carbon-supported Pt_1Cu_1 NDs (Pt_1Cu_1 NDs/C) showed 1.17 mA·cm^{-2} in area-specific activity, reaching an enhancement of ~5.32 times as compared with commercial Pt/C. In addition, Pt_1Cu_1 NDs/C maintained its superior ORR catalytic activity even after 12000 potential cycles during the accelerated degradation test, showing a remarkable electrochemical durability.

1 Experimental Section

1.1 Chemicals and Materials

Platinum (II) acetylacetonate [Pt(acac)$_2$, 97%], copper (II) acetylacetonate [Cu(acac)$_2$, 97%], oleylamine (OAm, 70%), acetic acid (> 99%) and perchloric acid ($HClO_4$, 70%) were all purchased from Sigma-Aldrich without further purification. Cetyltrimethylammonium bromide (CTAB, Aladdin, ≥ 99%), carbon black powders (AkzoNobel, EC-300J) and Nafion stock solution (DuPont, 20%) were all used as received. All aqueous solutions were prepared using ultrapure water (Millipore, > 18.2 MΩ·cm).

1.2 Preparation of Carbon-Supported Pt-Cu NDs

The uniform Pt-Cu NDs were synthesized through a one-pot process. In a typical synthesis, different amounts of Pt(acac)$_2$ and Cu(acac)$_2$ with the designed Pt/Cu atomic ratios were dissolved in 10 mL of OAm, followed by the addition of 295 mg of CTAB. The mixture was heated to 220 ℃ under air atmosphere with vigorous stirring, and then kept for 24 h. After cooling down, the as-synthesized Pt-Cu NDs were washed repeatedly by hexane and ethanol mixture, and then well-dispersed in chloroform. The carbon-supporting process was performed by mixing the Pt-Cu NDs suspension with a given amount of carbon black powders dispersed in chloroform. The product of Pt-Cu NDs/C was washed with ethanol repeatedly and precipitated by high-speed centrifugation. An acetic acid thermal treatment was applied to remove the residual organics on Pt-Cu NDs/C as reported in our previous work[1].

1.3 Characterizations

Transmission electron microscopic (TEM) and high-angle annular dark field scanning TEM (HAADF-STEM) images were all obtained on a JEOL JEM-ARM 200F spherical aberration correction transmission electron microscope. STEM energy dispersive X-ray spectroscopic (STEM-EDS) elemental analyses were also acquired on this device using the corresponding detector. The electron microscopic samples in this work were all prepared with Ni grids to avoid the Cu interference from Cu grids. X-ray diffraction (XRD) patterns were recorded on a Bruker D8 ADVANCE Da Vinci poly-functional X-ray diffractometer at a scan rate of 2 degree·min^{-1} with Cu K_α radiation (λ = 0.15404 nm). X-ray photoelectron spectroscopic (XPS) measurements were performed on a Shimadzu Kratos AXIS UltraDLD instrument. Inductively coupled plasma (ICP) elemental analyses were carried out with a Thermo iCAP7600 inductively coupled plasma-optical emission spectrometer (ICP-OES).

1.4 Electrochemical Measurements

All the electrochemical measurements in this work were conducted on a CHI660E potentiostat (Chenhua, Shanghai) with a conventional three-electrode system at room temperature. A saturated calomel electrode (SCE) coupled with a 1.0 mol·L^{-1} KNO_3 salt bridge was used as the reference electrode, while a 1 cm^2 platinum foil worked as the counter electrode. All the potentials in this paper are referenced to the reversible hydrogen electrode (RHE). The working electrode was prepared by pipetting a given amount of well-dispersed electrocatalyst ink onto a well-polished glassy carbon electrode (GCE, diameter: 5 mm). To activate the electrocatalysts, repeated potential cycling between 0 and 1.1 V in N_2-saturated 0.1 mol·L^{-1} $HClO_4$ solutions was applied at a scan rate of 100 mV·s^{-1}. Afterwards, steady cyclic voltammogram (CV) curves were acquired in fresh N_2-saturated 0.1 mol·L^{-1} $HClO_4$ solutions at a scan rate of 20 mV·s^{-1}, and the corresponding linear sweep

voltammogram (LSV) curves were then obtained in O_2-saturated 0.1 mol·L^{-1} $HClO_4$ solutions at a scan rate of 10 mV·s^{-1}. To evaluate the electrochemical durability, the accelerated degradation test (ADT) was conducted by performing repeated potential cycling between 0.7 and 1.0 V at a scan rate of 100 mV·s^{-1} in N_2-saturated 0.1 mol·L^{-1} $HClO_4$ solutions. CV and the corresponding LSV curves were recorded after every 6000 potential cycles. Electrochemical active surface area (ECSA) and ORR area-specific activity were calculated via the methods described in our previous report[1].

2 Results and Discussion

2.1 Synthesis and Characterization

Pt_3Cu_1 and Pt_1Cu_1 NDs were synthesized via a facile etching-based method. In this synthesis route, OAm worked as the solvent, reductant and stabilizer. CTAB was used as the capping and etching agent, which plays an important role in the formation of the dendritic morphology coupled with O_2.

As shown in Figure 1A and B, Pt_3Cu_1 and Pt_1Cu_1 NDs were uniform in both size and morphology. The average diameters of Pt_3Cu_1 and Pt_1Cu_1 NDs were 76.94 and 79.47 nm, respectively, and the corresponding relative standard deviations were only 11.2% and 5.9%. Figure 1C and D present the TEM images with higher resolution, in which the dendritic morphology can be clearly observed, showing etched multipods.

The compositions of Pt_3Cu_1 and Pt_1Cu_1 NDs were confirmed by the ICP-OES results. The Pt/Cu atomic ratio of Pt-Cu NDs can be easily tuned through varying the ratio of the Pt/Cu precursors. With the amount of $Cu(acac)_2$ being fixed at 0.05 mmol, the additions of 0.15 and 0.05 mmol of $Pt(acac)_2$ resulted in Pt_3Cu_1 and Pt_1Cu_1 NDs, respectively.

The composition distribution of Pt_1Cu_1 NDs was investigated by the STEM-EDS elemental mapping measurements. As presented in Figure 2A, the overlap image shows that the Cu and Pt signals almost distribute evenly, indicating the homogeneous alloy structure of Cu and Pt. The etched multipods can also

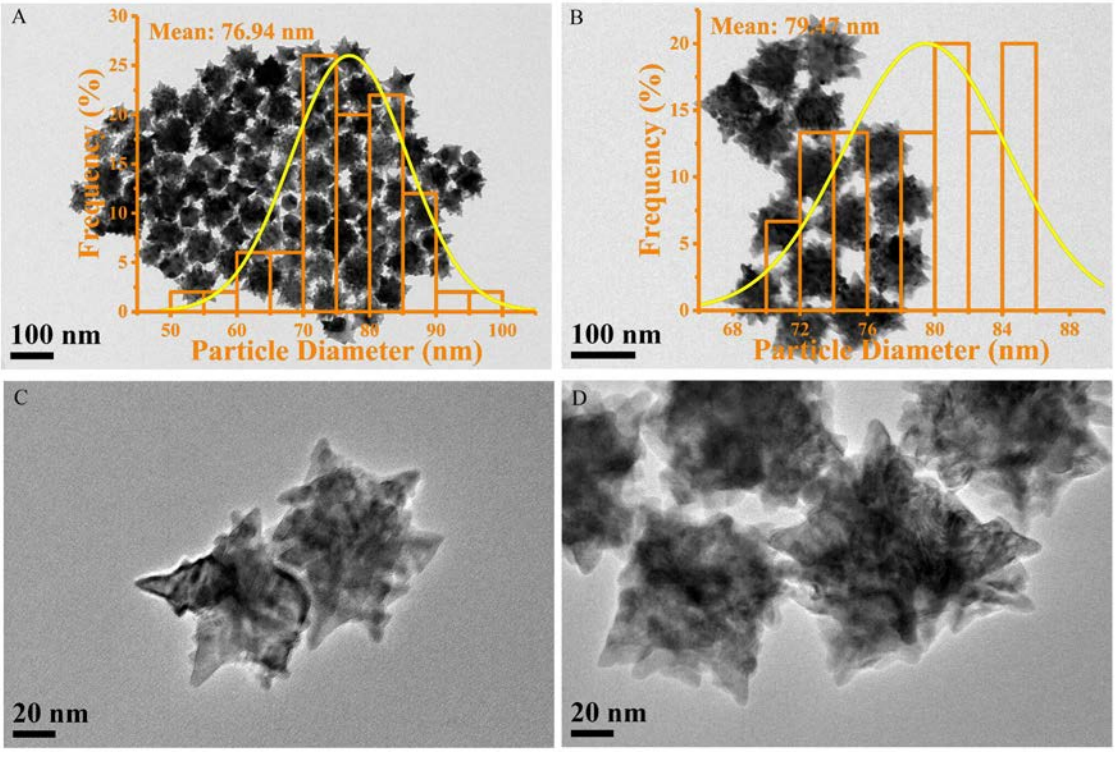

Fig. 1 Representative TEM images of (A, C) Pt_3Cu_1 and (B, D) Pt_1Cu_1 NDs. The insets are the corresponding histograms of particle diameter distribution.

be clearly observed in the HAADF-STEM image. In addition, to demonstrate the etching effect of the oxidative etchants of the Br^-/O_2 pair on the formation of the dendritic morphology, the intermediates sampled after 1 h reaction at different synthetic conditions were investigated. As shown in Figure 2B and C, the intermediates synthesized with the Br^-/O_2 pair were clearly etched and broken compared with those synthesized without Br^-/O_2 pair, which directly confirms the etching effect of the Br^-/O_2 pair. This etching effect was also observed previously[16].

XRD patterns in Figure 3 show that Pt_3Cu_1 and Pt_1Cu_1 NDs/C all possessed face-centered cubic (fcc) crystal structures with high crystallinities. It is worth noting that the diffraction peaks shifted toward higher 2 Theta angles with the increase of Cu content in Pt-Cu NDs/C, however, their peak positions fell between those of pure Pt and Cu. This can be attributed to the increased partial displacement of Pt atoms with Cu atoms based on Vegard's law, since the atomic radius of Cu (1.32 Å) is smaller than Pt (1.36 Å)[6, 17]. This upshift of diffraction peaks can lead to an increased surface lattice contraction of Pt-Cu NDs, and eventually results in an increased surface strain[1, 6, 10, 18-19]. Furthermore, the diffraction peak intensity ratios between (111) and (200) planes for Pt_3Cu_1 (2.52) and Pt_1Cu_1 (2.47) NDs are both higher than that (1.89) of the standard polycrystalline Pt, indicating that Pt_3Cu_1 and Pt_1Cu_1 NDs/C possess more {111} facets than polycrystalline Pt[6]. Such a structure can be attributed to the etched multipods of the dendritic morphology.

XPS measurements were made to probe the electronic structures of the electrocatalysts, as well as the d-band center shifting[1, 20]. The XPS spectrum of commercial Pt/C was obtained from our previous work and is included in the figure as a reference[1]. As presented in Figure 4, the binding energy (BE) of the Pt 4f clearly shifted toward higher energy as the Cu content increased in the electrocatalysts. The BEs of Pt $4f_{7/2}$ were 71.10, 71.40 and 71.62 eV for commercial Pt/C, Pt_3Cu_1 NDs/C and Pt_1Cu_1 NDs/C, respectively. The upshift of BE in Pt 4f indicates the electronic structure modification of Pt atoms in Pt-Cu NDs.

2.2 Electrocatalytic Property

The electrocatalytic properties of Pt_3Cu_1 and

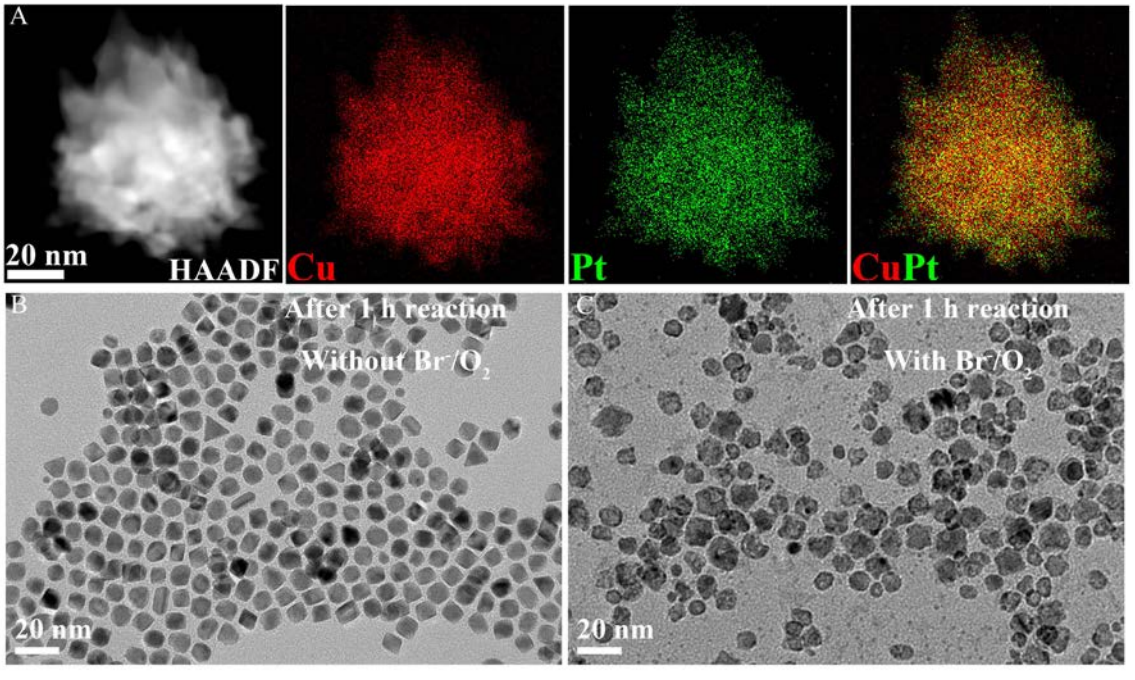

Fig. 2 (A) Representative STEM-EDS elemental mapping results of Pt_1Cu_1 NDs. Representative TEM images of the intermediates sampled after 1 h reaction (B) without and (C) with the oxidative etchants of the Br^-/O_2 pair.

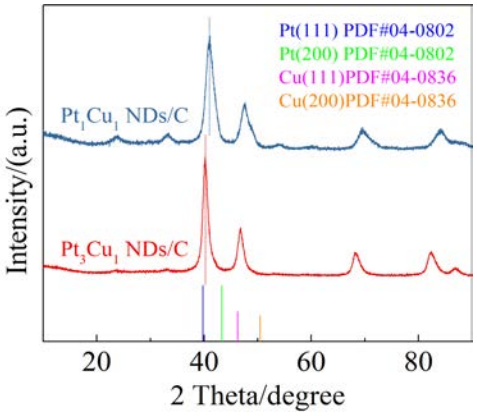

Fig. 3 XRD patterns of Pt_3Cu_1 and Pt_1Cu_1 NDs/C. The dotted lines represent the corresponding diffraction peak positions.

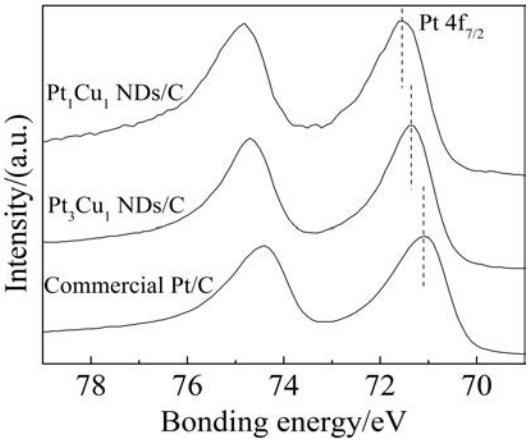

Fig. 4 XPS spectra of commercial Pt/C, Pt_3Cu_1 and Pt_1Cu_1 NDs/C. The dotted lines represent the corresponding peak positions.

Pt_1Cu_1 NDs/C were investigated and are compared with those of commercial Pt/C. Similarly, the electrocatalytic properties of commercial Pt/C obtained from our previous report were also used as a reference[1].

Figure 5A shows the Tafel plots for all the electrocatalysts in terms of area-specific activity, which are calculated without iR-correction or background-calibration. As presented in Figure 5B, Pt-Cu NDs/C exhibited significant enhancement compared with commercial Pt/C, thereinto, Pt_1Cu_1 NDs/C showed the highest area-specific activity of 1.17 mA·cm^{-2}, which is almost 5.32 times relative to that of commercial Pt/C. The composition-dependent enhancement of Pt-Cu NDs/C in ORR catalytic activity could be ascribed to the following factors. (1) The increased surface strain as indicated by the XRD patterns. (2) The modified electronic structures of Pt atoms as indicated by the XPS spectra. These two factors can both lead to a downshift of Pt d-band center, which can eventually cause a higher ORR catalytic activity[1, 6, 20]. (3) More {111} facets as revealed by the XRD patterns, which has been proved as the most active facets toward ORR among the low-index facets of Pt in $HClO_4$ solutions[9].

The electrochemical durability of Pt_1Cu_1 NDs/C is presented in Figure 5C and D. After 6000 and 12000 potential cycles during the ADT, the ECSAs of Pt_1Cu_1 NDs/C remained 99% and 96%, respectively, which are evidently higher than those (91% and 83%) of commercial Pt/C. The area-specific activities of commercial Pt/C only remained ~86% and ~77%, by contrast, the area-specific activities of Pt_1Cu_1 NDs/C increased to 1.22 and 1.23 mA·cm^{-2}, respectively, showing a remarkable electrochemical durability. Such an enhancement in ORR catalytic activity after the ADT could be attributed to the restructuring of Pt surfaces caused by the dissolution of Cu atoms, which was also observed in our previous report[1].

3 Conclusions

The composition-tunable Pt-Cu alloy NDs with uniform size and morphology were prepared via a facile etching-based process. It was found that the oxidative etchants of the Br^-/O_2 pair played an important role in the formation of the dendritic morphology. Benefiting from the combined effects of increased surface strain, modified electronic structure and active {111} facets, Pt-Cu NDs/C showed much higher area-specific activity toward ORR than commercial Pt/C. The most active Pt_1Cu_1 NDs/C exhibited the area-specific activity of 1.17 mA·cm^{-2}, which is ~5.32 times compared with commercial Pt/C. In addition, it also showed a remarkable electrochemical durability, preserving its superior activity even after 12000 potential cycles during the ADT. To optimize the ORR mass-specific activity of Pt-Cu NDs/C, future work

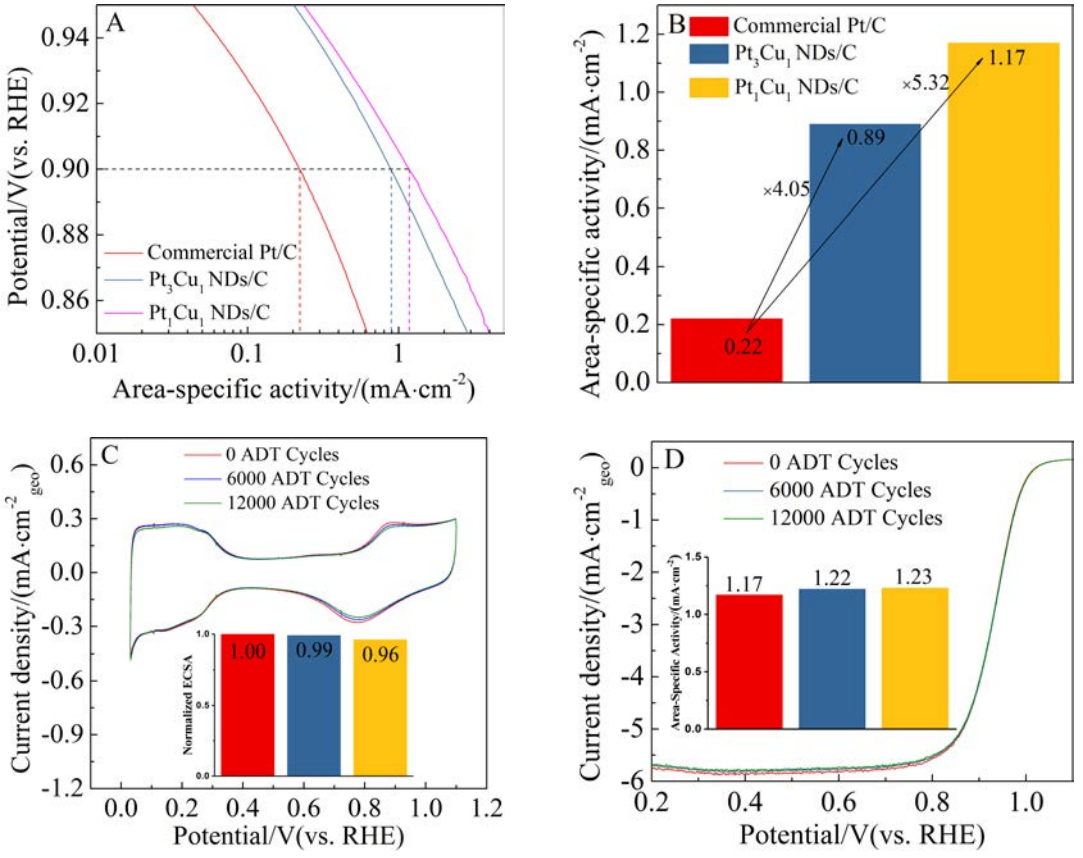

Fig. 5 (A, B) ORR catalytic activities (Tafel plots) of commercial Pt/C, Pt_3Cu_1 NDs/C and Pt_1Cu_1 NDs/C. Evolution of (C) CV and (D) LSV curves for Pt_1Cu_1 NDs/C.

will focus on reducing the particle size of Pt-Cu NDs through adjusting the synthetic condi tions, such as heating temperature, reaction time, precursor concentration, and so on.

Acknowledgements

This work was funded by the National Key Research and Development Program of China (No. 2016YFB0101201) and the National Natural Science Foundation of China (No. 21533005 and No. 21503134).

References:

[1] Luo L X, Zhu F J, Tian R X, et al. Composition-graded Pd_xNi_{1-x} nanospheres with Pt monolayer shells as high-performance electrocatalysts for oxygen reduction reaction[J]. ACS Catalysis, 2017, 7(8): 5420-5430.

[2] Chen A C, Holt-Hindle P. Platinum-based nanostructured materials: synthesis, properties, and applications[J]. Chemical Reviews, 2010, 110(6): 3767-3804.

[3] Debe M K. Electrocatalyst approaches and challenges for automotive fuel cells[J]. Nature, 2012, 486(7401): 43-51.

[4] Wang Y J, Zhao N N, Fang B Z, et al. Carbon-supported Pt-based alloy electrocatalysts for the oxygen reduction reaction in polymer electrolyte membrane fuel cells: particle size, shape, and composition manipulation and their impact to activity[J]. Chemical Reviews, 2015, 115(9): 3433-3467.

[5] Cheng N C, Banis M N, Liu J, et al. Extremely stable platinum nanoparticles encapsulated in a zirconia nanocage by area-selective atomic layer deposition for the oxygen reduction reaction[J]. Advanced Materials, 2015, 27(2): 277-281.

[6] Wu J B, Gross A, Yang H, et al. Shape and composition-controlled platinum alloy nanocrystals using carbon monoxide as reducing agent[J]. Nano Letters, 2011, 11(2): 798-802.

[7] Zhang J L, Vukmirovic M B, Xu Y, et al. Controlling the catalytic activity of platinum-monolayer electrocatalysts for oxygen reduction with different substrates[J]. Angewandte Chemie International Edition, 2005, 44 (14): 2132-2135.

[8] Tian R X, Shen S Y, Zhu F J, et al. Icosahedral Pt-Ni

nanocrystalline electrocatalyst: growth mechanism and oxygen reduction activity[J]. ChemSusChem, 2018, 11(6): 1015-1019.

[9] Stamenkovic V, Markovic N M, Ross P N. Structure-relationships in electrocatalysis: oxygen reduction and hydrogen oxidation reactions on Pt(111) and Pt(100) in solutions containing chloride ions[J]. Journal of Electroanalytical Chemistry, 2001, 500(1/2): 44-51.

[10] Koenigsmann C, Santulli A C, Gong K P, et al. Enhanced electrocatalytic performance of processed, ultrathin, supported Pd-Pt core-shell nanowire catalysts for the oxygen reduction reaction[J]. Journal of the American Chemical Society, 2011, 133(25): 9783-9795.

[11] Lim B K, Jiang M J, Camargo P H C, et al. Pd-Pt bimetallic nanodendrites with high activity for oxygen reduction[J]. Science, 2009, 324(5932): 1302-1305.

[12] Lim B K, Jiang M J, Yu T K, et al. Nucleation and growth mechanisms for Pd-Pt bimetallic nanodendrites and their electrocatalytic properties[J]. Nano Research, 2010, 3(2): 69-80.

[13] Si W F, Li J, Li H Q, et al. Light-controlled synthesis of uniform platinum nanodendrites with markedly enhanced electrocatalytic activity[J]. Nano Research, 2013, 6(10): 720-725.

[14] Zhang G, Shao Z G, Lu W T, et al. One-pot synthesis of Ir@Pt nanodendrites as highly active bifunctional electrocatalysts for oxygen reduction and oxygen evolution in acidic medium[J]. Electrochemistry Communications, 2012, 22: 145-148.

[15] Wang L, Yamauchi Y. Autoprogrammed synthesis of triple-layered Au@Pd@Pt core-shell nanoparticles consisting of a Au@Pd bimetallic core and nanoporous Pt shell[J]. Journal of the American Chemical Society, 2010, 132(39): 13636-13638.

[16] Luo S P, Shen P K. Concave platinum-copper octopod nanoframes bounded with multiple high-index facets for efficient electrooxidation catalysis[J]. ACS Nano, 2016, 11(12): 11946-11953.

[17] Cordero B, Gomez V, Platero-Prats A E, et al. Covalent radii revisited[J]. Dalton Transactions, 2008, 21: 2832-2838.

[18] Gan L, Heggen M, Rudi S, et al. Core-shell compositional fine structures of dealloyed Pt_xNi_{1-x} nanoparticles and their impact on oxygen reduction catalysis[J]. Nano Letters, 2012, 12(10): 5423-5430.

[19] Adzic R R, Zhang J L, Sasaki K, et al. Platinum monolayer fuel cell electrocatalysts[J]. Topics in Catalysis, 2007, 46(3/4): 249-262.

[20] Wakisaka M, Mitsui S, Hirose Y, et al. Electronic structures of Pt-Co and Pt-Ru alloys for CO-tolerant anode catalysts in polymer electrolyte fuel cells studied by EC-XPS[J]. The Journal of Physical Chemistry B, 2006, 110(46): 23489-23496.

Pt-Cu 合金纳米枝晶的合成及其氧还原催化性能

罗柳轩[1]，魏光华[2]，沈水云[1]，朱凤鹃[1]，柯长春[1]，闫晓晖[1]，章俊良[1*]

（1. 上海交通大学机械与动力工程学院燃料电池研究所，动力机械与工程教育部重点实验室，上海 200240；
2. 上海交通大学巴黎高科卓越工程师学院，上海 200240）

摘要： 纳米材料的结构和化学成分对其催化性能的显著影响已经得到验证. 因此，本文通过一种简易的蚀刻方法，合成出具有均匀合金结构且尺寸和形貌均一的 Pt-Cu 纳米枝晶（NDs）作为高效氧还原（ORR）催化剂. 其树枝状形貌的形成得益于由 Br^-/O_2 氧化蚀刻剂引起的蚀刻效应. 通过改变 Pt/Cu 前驱体的比例可以容易地调节 Pt-Cu NDs 的 Pt/Cu 原子比，而不会使其树枝状形貌发生改变. 活性最高的碳载 Pt_1Cu_1 NDs（Pt_1Cu_1 NDs/C）的面积比活性为 1.17 $mA\cdot cm^{-2}$@0.9V（vs. RHE），约为商业 Pt/C 的 5.32 倍. 此外，Pt_1Cu_1 NDs/C 还具有卓越的电化学耐久性，即使在经过加速衰减实验的 12000 个电势循环后仍保持其优异的 ORR 催化活性. Pt_1Cu_1 NDs/C 优异的 ORR 催化活性和电化学耐久性得益于由其合金结构和枝晶形貌产生的电子效应和结构效应.

关键词： 铂；合金；电催化剂；纳米枝晶；氧还原